Structure Analysis of Some Fused Materials by X-ray Diffraction : Part I. $NaNO_3$, $NaNO_2$ and PbO-B_2O_3 System

Structure Analysis of Some Fused Materials by X-ray Diffraction

Part I. $NaNO_3$, $NaNO_2$ and PbO-B_2O_3 System*

Kazuo FURUKAWA

The Research Institute for Iron, Steel and Other Metals

(Received February 8, 1960)

Synopsis

A new method of X-ray diffraction measurement widely applicable to fused materials including corrosive substances up to high temperature ranges has been described. By the Fourier Analysis of X-ray diffraction data, the atomic radial distribution curves of several fused materials have been obtained. Fused $NaNO_3$ and $NaNO_2$ contain Na^+ ions and NO_3^- or NO_2^- radicals, which are in thermal motion being restricted by their specific shapes and charge distributions. The structure of fused PbO-B_2O_3 system in the range of $PbO/B_2O_3 = 4/1$ to $1/3$ in mol-ratio are, in general, considerably similar to their glass, but Pb-O bonds become more ionic by the fusion or by the increase of B_2O_3 content. Its abnormal glass-forming-limit (94 wt % in PbO) is also explained.

I. Introduction

With the aim of clarifying the physical properties of fused salts and slags, physico-chemical studies have been performed from many stand points, but the lack of knowledge of liquid structure has offered a fundamental impediment to clarify the essential features of fused state. So, in order to obtain direct informations on the atomic arrangements of liquids, the structure analysis by means of diffraction of X-ray, electron- or neutron-beam have been undertaken, but the tremendous difficulties in the experimental applications of these methods have hampered their wide exploitation.

The principle of X-ray structure analysis of polyatomic liquids has been established by B. E. WARREN et al. already in 1936 and first applied to studies on glasses,(1) but its applications to fused salts and oxides have only lately been begun. As far as we could ascertain, there have been research works in the field by R. E. WOOD, H. L. RITTER et al. on halides of low-melting point such as $AlCl_3$, InI_3, SnI_4 and CdI_2 by means of the capillary shielding method(2); the

* The 974th report of the Research Institute for Iron, Steel and Other Metals.
This paper was read at the "International Symposium on the Physical Chemistry of Process-Metallurgy," Pittsburgh, U. S. A. (1959, April).

(1) B. E. Warren, H. Krutter and O. Morningster, J. Am. Cer. Soc. **19** (1936), 202; B. E. Warren, ibid., **24** (1941), 256.

(2) R. L. Harris, R. E. Wood and H.L. Ritter, J. Am. Chem. Soc. **73** (1951), 3151; R. E. Wood and H. L. Ritter, ibid., **74** (1952), 1760, 1763; **75** (1953), 471.

work of Prof. KORA et al. on several halides by the same method[3]; the study on KNO_3 and $NaNO_3$ by the same method in USSR[4]; measurements on alkali-halides[5] (m.p. $<$ 665°C), sealed in the Beryllium cup; measurements on several halides (including high melting point compounds) by penetration of X-ray through films of the specimen liquids suspended in slits made of heating materials themselves[6] and studies of H. RICHTER et al. on glassy and fused B_2O_3[7].

Independent of these studies, we have been working toward establishing a measuring method of our own for the structure analysis of liquid metals and complex fused oxides for several years, as reported in the following together with a few examples of its practical application.

II. Experimental

(A) Apparatus

a) Sample case

The penetrating power of X-ray is not so high enough that absorption correction cannot be accurately carried out, when glass or quartz tubes are used for sealing of the molten specimens (Be is the only exception). Besides, these materials are unsuitable for specimens of high melting point or of corrosiveness. Therefore, as a container we used dishes made of the noncorrosive materials such as fused alumina, graphite or platinum etc., and adopted the method of measuring the reflection from the free surface of liquid. The fused materials being apt to wet the dish and overflow its brim, thus damaging the heater, lead-edges provided on both sides of the dish and any fused material spilled was collected in two receptacles beside the dish.

The heater was of platinum-rhodium wire wound reciprocally up and down for preventing electrolysis of accidentally spilled salts (cf. Fig. 1).

These were placed in a square box of stainless steel and covered with a semicylindrical lid of stainless steel. The lid was 12 cm in diameter and had a window of 15 mm in breadth and extending over 180° at the center of lid, on which aluminium foil was stretched, to admit entrance and exit of X-rays. The position of the dish and Pt-furnace could be regulated up and down with micro-screws from the outside of the case-

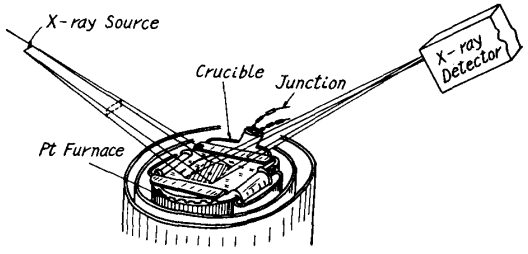

Fig. 1. Arrangement of X-ray Apparatus.

(3) K. Kora et al., Read at the Meeting of the Physical Society of Japan (1951) (1952).
(4) V. I. Danilov and S. Ya Krasnitskii, Dokl. Akad. Nauk. USSR **101** (1955), 661.
(5) P. A. Agron, M. D. Danford, M. A. Bredig, H. A. Levy and P. C. Sharrah, Acta Crys. **10** (1957), 739, Abstract of papers of "Int. Union of Crys: 4th Int. Congress"; M. D. Danford, P. A. Agron, M. A. Bredig and H. A. Levy, ibid., 829. (The principle of their method seemingly happens to be similar to ours.)
(6) J. Zarzycki, J. Phys. Rad. (Suppl. Phys. Appl.) **18** (1957) 65A; **19** (1958), 13A.
(7) F. Herre and H. Richter, Z. Naturforsch. **12a** (1957), 545.

box and its total surface was water-cooled. For keeping the atmosphere in the case inert and preventing sublimation of the sample on the window of the lid, dry nitrogen gas was introduced through a jet beside the window.

b) Goniometer

For measuring the diffraction from a free liquid surface, it is advantageous that the X-ray detector are symmetrically moved at an equal velocity with a horizontal axis passing along the liquid surface, for this assures the condition of the parafocussing arrangement (Fig. 1 and Photo. 1.)

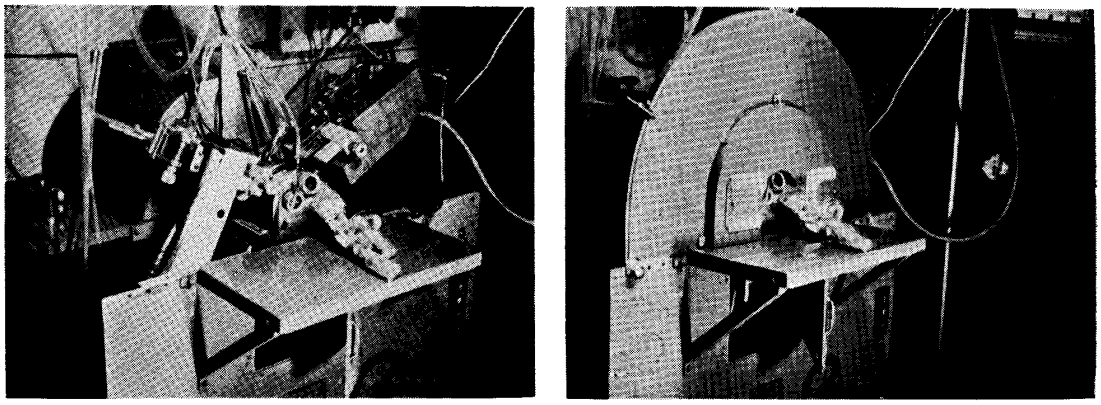

a b

Photo 1. X-ray diffractometer

c) X-ray Source

A philips X-ray tube with Cu target was used. The primary A.C. supply voltage was stabilized within a ±0.1 per cent at 200 Volts and the fluctuation of the electron beam current in X-ray tube was kept within ±0.2per cent by feeding it back into the filament current through a saturable reactor.

d) X-ray Detector

A Kr-filled proportional counter was used. The channel width of the pulse-height analyzer was kept equal to the half-maximum width of Cu $K\alpha$, and $K\beta$ and the residual white-X-ray were eliminated using Ni-Co differential filters carefully adjusted. The intensity distribution of the effective X-ray was as shown in Fig. 2.

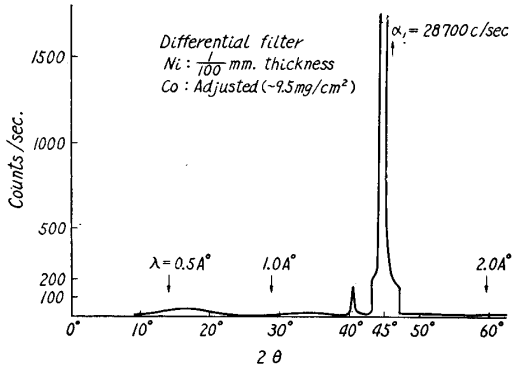

Fig. 2. Intensity distribution of monochromatized X-ray (Cu $K\alpha$) using balanced filters and pulse-height analyzer.

(B) Measurements

The crucible was placed on the furnace so that the two lead-edges were level horizontally, and filled with the molten sample not so much as to cause overflow of the melt. The level of surface was regulated by a screw beneath the furnace so as to coincide nearly with the central axis of the goniometer. Then the goniometer was moved up and down, and recording the X-ray scattering intensity curve on the automatic recorder-

chart the height of the liquid surface was adjusted by a microscrew so that the largest peak in the intensity curve was higher as much as possible. After these adjustments the projected measurement was begun.

Before and after every round of measurement, the height of the liquid surface was checked and if a perceptible change was found, the measured value was rejected. When required, the sample was replenished through a special supplier from outside, to make up its loss.

The determination of temperature on the surface of the liquid is very difficult, but since the melting point can be defined as the point where the sharp patterns of the X-ray scattering curve, essential characteristics to the crystal powder, disappear, we made our measurements usually at a temperature higher by 5–10°C above the melting point as measured by a Pt–PtRh junction.

The measured angles ranged between 10° and 140° in diffraction angles. As the flat area on the free liquid surface was about 20×20 mm, slit-widths of collimators were selected that were adapted to the diffraction angle.

The rotation of the goniometer was kept at first at the rate of about 2° per minute for determining the general outline of the scattering intensity curve as shown in Photos. 2 and 3, then it was slowed down to about $\frac{1}{2}$° per min. for precise measurement of several portions of the intensity curves. The average of the reliable values obtained by three measurements was adopted as a correct value. The intensity ratio due to the use of Ni-filter and Co-filter was checked before and after every measurement.

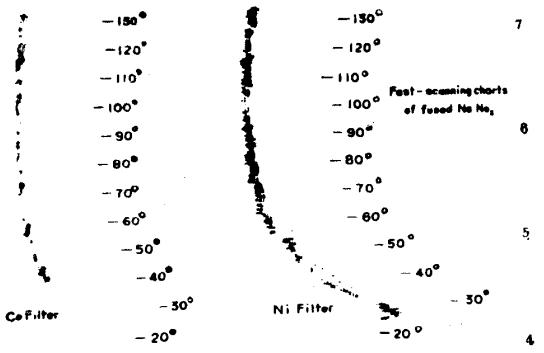

Photo. 2. Fast scanning chart of fused $NaNO_2$

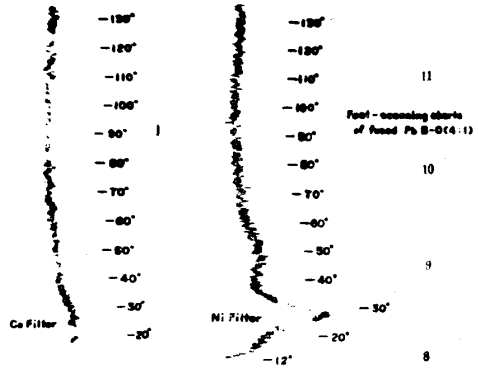

Photo 3. Fast scanning chart of fused PbO-B_2O_3 (4 : 1)

(C) Calculations

After the polarization-correction of the measured values they were analysed by the standardized procedure[1], by which the average radial distribution of the electron density around the atoms per molecule may be given by the next formula:

$$4\pi r^2 \cdot \sum_m \cdot \bar{K}_m \cdot g_m(r)$$

$$= 4\pi r^2 \cdot g_0 \sum_m K_m + \sum_m (K_m)^2 \cdot \frac{2r}{\pi} \int_0^\infty s \cdot i(s) \cdot \sin rs \cdot ds.$$

r = distance from any atom
$\bar{K}_m$ = effective number of electrons in the atom m
$g_m(r)$ = effective electron density at a distance r from the atom m
g_0 = average electron density
$s = 4\pi \sin\theta/\lambda$ $\quad 2\theta$ = diffraction angle
λ = wave-length of X-ray
$i(s)+1 = I_{\text{CO.}}/I_{\text{indep. coh.}}$
$I_{\text{CO.}}$ = dependent coherent scattering intensity
$I_{\text{indep. coh.}}$ = independent coherent scattering intensity (theoretically calcurable)

For determining $\bar{K}_m$, the scattering factors different by the electronic states of atoms must be used[8], but since the analytical results are practically similar whether the neutral or the ionic state is assumed, the calculations in the following have been done always under assumption of ionic states.

For determining I_{CO} from experimental values there are two applicable methods. The one is in postulating that this value is equal to $I_{\text{indep. coh.}}$ in the range of large s-value and other is in utilizing the fact that at $r=0$, $g_m(0)=0$, which justifies rewriting the formula (1) as

$$\int_0^{s_{\max}} s^2 \cdot i(s) \cdot ds = -2\pi^2 \cdot g_0 \cdot \frac{\sum_m \bar{K}_m}{\sum_m (\bar{K}_m)^2} \qquad (2)$$

and thus $i(s)$ is determined by the trial and error method. In the cases with $NaNO_3$ and $NaNO_2$ mentioned below, the latter method was more effective.

In our case, $s_{\max}$ was 7.5 and assuming $\Delta s \times \frac{10}{\pi} = 0.3$, we obtained 80 values of $i(s)$ and carried out the FOURIER summation of formula (1) by the help of the Parametron-electronic computer (P.C. 1) at the Department of Physics, University of Tokyô.

Due to the termination effect and other factors there is the fear of various ghosts appearing in the radial distribution curves thus obtained[9], calling for careful examination and experimental reconfirmation. So, the subtotal was taken up or $[I_{\text{CO}} - I_{\text{indep. coh.}}]$ was substituted[9] into $i(s)$ in the integral in (1) to check the calculations. These FINBAK's integration values in the cases of $NaNO_3$ and $NaNO_2$ are given in collation in Figs. 4 and 6.

III. Results and Discussions

The results of application of the above method described in our studies on the fused salts or fused oxides having radicals are reported hereunder.

In the first place, substances containing $(NO_3)^-$ or $(NO_2)^-$ radicals were taken up as examples with the simple radicals. Next, as an example of fused borates

(8) J. Berghuis et al., Acta Crys. **8** (1955) 478; Viervoll and Ögrim, ibid., **2** (1949) 277; "Intern. Tab. of Det. Crys. Struc." (1938).
(9) C. Finbak, Acta Chem. Scandina. 3 (1949), 1279, 1293; O. Borgen and C. Finbak, ibid., **8** (1954), 829.

the Pb–B–O system was taken up.

(A) Fused Sodium Nirate and Nitrite

These are compounds very suitable for our experiment, having low melting points, but it is known that the nitrates are apt to be decomposed into nitrites by

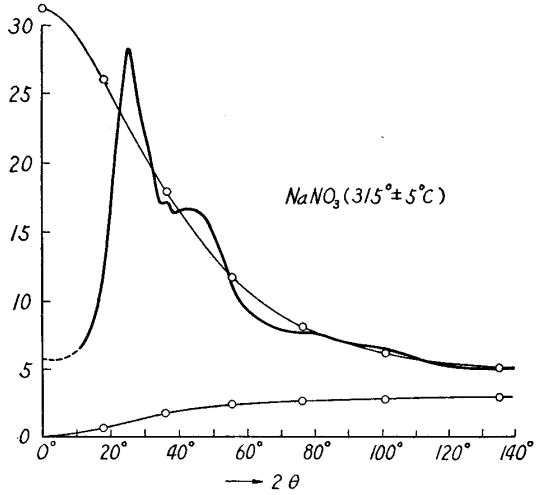

Fig. 3. X-ray scattering intensity curve of fused $NaNO_3$.

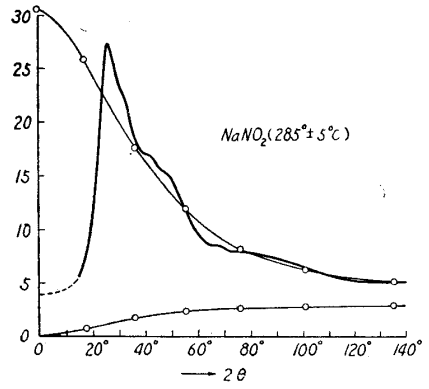

Fig. 5. X-ray scattering intensity curve of fused $NaNO_2$.

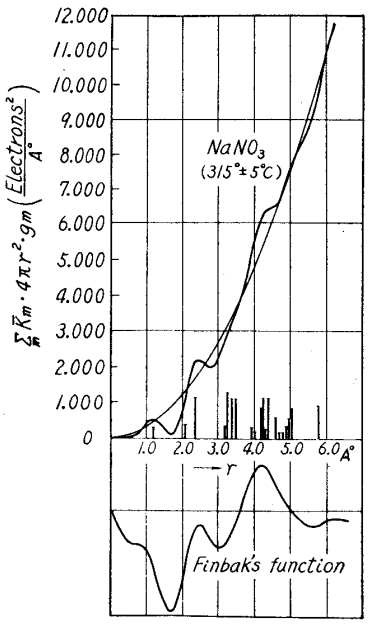

Fig. 4. Radial distribution curve of fused $NaNO_3$.

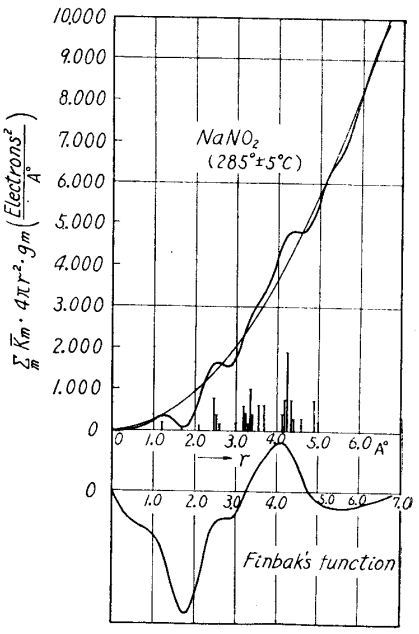

Fig. 6. Radial distribution curve of fused $NaNO_2$.

X-ray.[10] In our experiments, however, the crucible was made sufficiently large to minimize the effect of change in the liquid surface level and the volume exposed to X-ray was on the average below about 1/10 of the total volume of the specimen, so that the quantity of nitrite produced during the experiment can be inferred to be less than 1 per cent of the total and thus negligible in our computations.

The corrected scattering intensity curves of $NaNO_3$(m.p. 308°C) and $NaNO_2$

(10) G. Henning, R. Lees and M.S. Matheson, J. Chem. Phys. **21** (1953), 664; J. Cunningham and H.G. Heel, Trans Farad. Soc. **54** (1958), 1355.

(m.p. 277°C) at 315±5°C and 285°±5°C respectively, and the radial distribution curves obtained by applying FOURIER analysis to them are shown in Figs. 3~6. The measured densities by BLOOM et al.[11] were adopted as the values required in the computations.

a) **$NaNO_3$**

This compound is in the form of rhombohedral crystals,[12] rather resembling those of NaCl and the ionic radii of Cl^- and NO_3^- are nearly equal *i.e.* 1.81Å and 1.89Å respectively, but interesting enough, their melting points are much different.[13]

The shape of NO_3^- is of an equilateral triangle and the distance N-O =1.21Å and O-O=2.1Å, perhaps owing to the resonance of the three electronic structures as follows:[14]

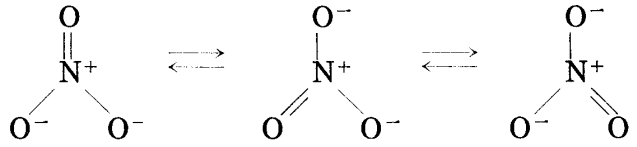

Therefore, on the average, N and O may be assumed to have the electric change distribution of $+1$ and $-\frac{2}{3}$ respectively. NO_3^- are said to begin above 185°C the rotational vibration violently, and to perform above 280°C the free rotation around the triple axes.[15]

Assuming the electronic structure of Na^{+1}, N^{+1} and $O^{-\frac{2}{3}}$ in molten state too, the result of our analysis is Fig. 4. In this case, we have $\bar{K}_{Na}=12.1$, $\bar{K}_O=7.8$ and $\bar{K}_N=6.2$.

The first peak in the curve is located at 1.25Å and is due to the interference of scattering from N and O ions, for short, the N-O interference. The coordination number n of oxygen around nitrogen is

$$n=\frac{272}{2\times\bar{K}_N\times\bar{K}_O}=2.81\approx 3,$$

and correspounds approximately with that of NO_3 radical. The O-O interference peak that should be located at 2.1Å is observed to be overlapping with another peak. These findings show that NO_3^- exists in the melt too.

The arrangement of ions in the crystal is shown by the column-graph in Fig. 4, but the correlation between it and the radial distribution curve is not clear enough and the relation between NO_3^- and Na^+ ions in the melt must be further discussed.

Taking the ionic radius of Na^+ as 0.95Å, nitrogen and oxygen are calculated as having the contact radii of 1.5Å and 1.4Å respectively, as illustrated in Fig. 7 and as the more probable arrangements of Na^+, the four models of A, B, C and D

(11) H. Bloom, I.W. Knaggs, J.J. Molley and D. Welch, Trans. Farad. Soc. 49 (1953), 1458.
(12) R.W.G. Wyckoff, "Crystal Structure" (1948).
(13) W.J. Davis, S.E. Rogers and A.R. Ubbelohde, Proc. Roy. Soc. **A220** (1953), 14.
(14) L. Pauling, "Nature of Chemical Bonds" (1940).
(15) J.M. Bijvoet and J.A.A. Kelelaar, Phys. Rev. **54** (1934), 625.

may be proposed, which have many equivalent points. The ratio of static potentials among the four cases may be computed as $-0.313 : -0.371 : -0.358$, so the positions B and D and their equivalents may be known to be more stable than the other two. [In the crystal at low temperature, Na^+ stands in an intermediate position between A and D.]

On the other hand, if NO_3^- is in perfect free rotation, it would occupy a sphere-volume of 2.61Å radius and if such spheres are closest-packed with Na^+ ions of 0.95Å radius, the density would fall about 20 per cent lower than the actual density, so that a completely free rotation of NO_3^- in melt was not proved.

From the above results, we have been led to adopt something as follows as the configurational model of fused $NaNO_3$; the Na^+ and NO_3^- ions of definite sizes and shapes, though they may take complicately different mutual positions owing to the thermal motion, take most frequently such positions as given by B, and D in Fig. 7 and their equivalent positions.

By this model, we could expect a large peak at or near 2.35Å due to the interference from Na^+ and the two oxygen ions in contact therewith. This distance may be increased somewhat owing to the thermal agitation and this is in surprising coincidence with the second peak at 2.45Å.

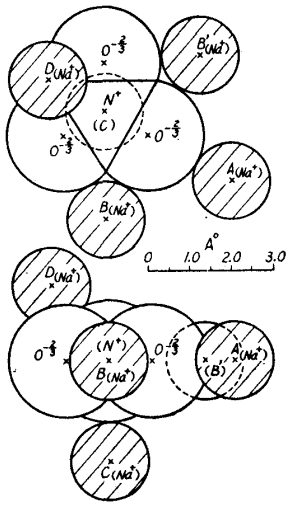

Fig. 7. Orientations of NO_3^- and Na^+ ions.

Next, in the case when two NO_3^- radicals are in near approach to one Na^+, the mutual electrostatic repulsion between two NO_3^- ions will cause the two to take positions on opposite sides of Na^+, but every NO_3^- ion may be in rotation around the principal axis, the line through Na^+ and two nitrogen ions, so that the largest peak will appear at 4.2–4.7Å (mean value : 4.45Å) owing to the interference O_2–O_2, which denotes the interference between two sets of two oxygen ions of each NO_3^- radical in contact with Na^+. But if such normal opposite positions are agitated by thermal motion, the distance between them would be somewhat shortened. This expected peak is seen to match exactly the third peak. In such groupings, however, another model using position C above cannot be altogether neglected, for even if the probability of such a position is smaller, the interference between two sets of three oxygen ions of each NO_3^- ion is not so weak, because its intensity per pair of NO_3 would be $\frac{3\times3}{2\times2}$ or 2.25 times as large as that of interference O_2–O_2. This would cause a peak at 5.0–5.6Å. In Fig. 4, we see a weak peak satisfying this anticipation.

Next, we will take up the case where two Na^+ ions come near one NO_3^-. In such a case, the largest peak will be that due to the Na–Na interference, and if we consider that the distance Na(B-position)–Na(B-positition) equals to 4.75Å,

Na(B)–Na(D) to 4.2Å and Na(D)–Na(D) to 4.7Å and that intermediate positions between the three occur, the peak due to such interferences will also come very near to the third peak. But the peak intensity of this interference is smaller than that of O_2–O_2 interference, being $(12.1)^2/(2\times7.8)^2$ or about 60 per cent of the latter.

Secondary interferences besides the above may occur, but these can form only weak peaks than the above, so that we need not give here detailed accounts of them.

In short, it has been demonstrated that our model postulated upon reliance on the shape and the electrostatic forces of ions is a very effectively serviceable model. Such a specific configuration as shown in our model causes to bring about an excess configurational entropy to the melt, which causes in turn, as UBBELOHDE et al.[13] have already pointed out, that nitrates have lower melting points than chlorides of the same cations, for the melting point T_m can be determined by

$$T_m=\frac{\Delta H_m}{\Delta S_m},$$

ΔH_m : heat of fusion

ΔS_m : entropy of fusion

so that, if ΔH_m is not widely different from that of chlorides, the larger the ΔS_m, the lower the T_m. It is said that abnormal properties of nitrates result from the existence of association complexes in them, but the abnormal excess entropy and others of nitrates should be interpreted by only our dynamical model.

b) $NaNO_2$

The crystal of $NaNO_2$ has an orthorhombic structure,[16] similar to the NaCl type structure also. Its NO_2^- radical has the angle $\angle$O–N–O=115.4° the distance N–O=1.236Å and O–O=2.10Å, and its electronic structure may be understood as follows:

Therefore, taking the mean electric charge of nitrogen as zero and that of oxygen as $-\frac{1}{2}$, the results of analysis were shown in Fig. 6. In this case, we have $\overline{K_{Na}}=12.08$, $\overline{K_0}=7.76$ and $\overline{K_N}=6.39$

The presence of NO_2^- radicals has been confirmed by the appearance of the first peak. This shows that the coordination number n of oxygen is

$$\frac{196}{2\times\overline{K_0}\times\overline{K_N}}=1.98\approx2.$$

Upon comparison of the curve in Fig. 6 with the atomic distribution in the crystal (the column graph in Fig. 6), a somewhat better correlation is observed than in the case with $NaNO_3$, perhaps owing to the electro-neutrality of nitrogen and the simplershape of NO_2^-.

But in this case too, a model similar to that of fused $NaNO_3$ above was found

(16) G.B. Carpenter, Acta Crys. **5** (1952), 132; **8** (1955), 852.

very effective. The more probable orientation models of NO_2^- radicals and Na^+ ions are shown in Fig. 11, in which the ratio of electrostatic potentials of Na^+ at the positions A, B, C and D is $-0.425 : -0.425 : -0.294 : -0.346$. And as the neutrality of nitrogen readily suggests, the positions A, B and B′ including their intermediates are the most stable. [In the crystal, position A is occupied.]

Accordingly, the model of fused $NaNO_2$ has been assumed as follows; the NO_2^- radicals and Na^+ ions in fused $NaNO_2$ take different compliated mutual orientations owing to thermal motion, but the most probable positions are these near B, A and B′ and their intermediates in Fig. 8.

When such a model is adopted, some interference is expected from Na^+ and two oxygen of NO_2^- in contact with it, and this is precisely reflected by the second peak in Fig. 6., as was in the case with $NaNO_3$.

In the case when two NO_2^- are adjacent to a Na^+, the O_2–O_2 interference becomes the same as in $NaNO_3$ and the third peak in Fig. 6 here too definitely shows the existence of this interference.

In the case when two Na^+ are near a NO_2^-, the arrangement would be Na(B-position)–Na(B′-position) with a distance of 4.1Å or near, which is the value included in the range of the extension of the third peak on the short distance side.

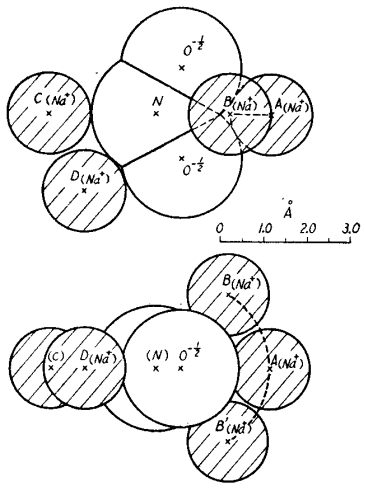

Fig. 8. Orientations of NO_2^- and Na^+ ions.

As previously stated, if the distribution closer resembling that of the crystal is also taken as possible and reasonable than in the case of $NaNO_3$, the elevated part of the curve in the vicinity of 3.5Å can be readily explained (see column graph in Fig. 6).

(B) PbO–B_2O_3 system

We are at present in the course of examining the structure of fused silicates and fused borates, and as one of them we have taken up the Pb–B–O system, which has the low melting point below 800°C in all compositions (Fig. 9), and have been subjected to physico-chemical researches in many aspects. Besides, borates and silicates usually have complex structures so that the peaks in their radial

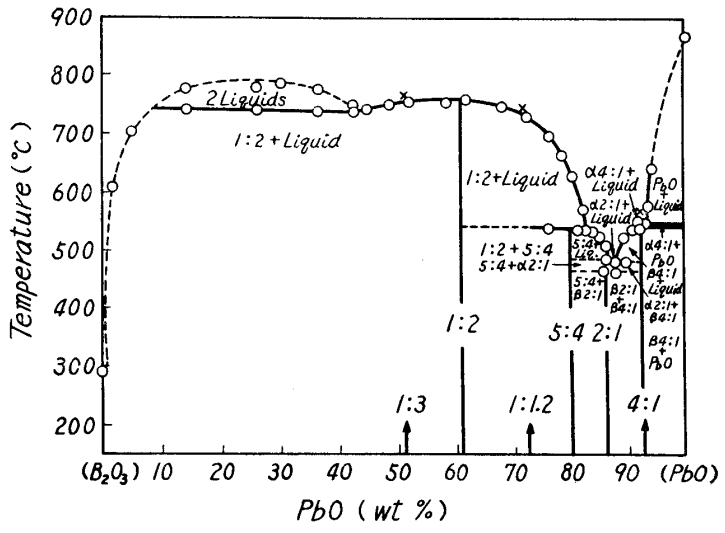

Fig. 9. Phase diagram of PbO–B_2O_3 [From R.E. Geller and E.N. Bunting: J. Res. Nat. Bur. Standard, **18** (1937) 585].

distribution curves are frequently overlapped with one another, causing difficulty in analyzing them, but in the Pb–B–O system the scattering factor of Pb is overwhelmingly predominant, so that the peaks due to Pb are very easy to discriminate from these due to the other elements. For example, in the case of the mol-ratio PbO/B_2O_3 is 4/1, the atom-ratio Pb/B is 2 and $(\bar{K}_{Pb})^2/(\bar{K}_B)^2$ is 1,125, so the actual ratio of a peak area of Pb–Pb interference to that of B–B amounts to the height of 4,500; even when PbO/B_2O_3 is 1/3, the ratio is 22.4. [But we must point out that the peaks concerning with oxygen ions cannot be neglected in the region of lower content of PbO, for example, we have

$$\frac{\bar{K}_{Pb}}{\bar{K}_0} = 14 \text{ and } \frac{N_{Pb}}{N_0} = \frac{1}{10} \text{ at } \frac{PbO}{B_2O_3} = 1/3,$$

becoming the contributions of Pb and O comparable (cf. Tab. 1).]

Table 1. Compositions and Effective electron numbers of Pb—B—O.

Mol-ratio $PbO : B_2O_3$		Atom-ratio Pb : B : O	Ratio of Effective electron numbers $\bar{K}_{Pb^{++}} : \bar{K}_{B^{+++}} : K_{O^{--}}$	PbO wt.%
4 : 1	$(PbO)_{0.8}$ $(B_2O_3)_{0.2}$	0.8 : 0.4 : 1.4	85.9 : 2.56 : 6.51	92.8%
1 : 1.2	$(PbO)_{0.455}$ $(B_2O_3)_{0.545}$	0.455 : 1.09 : 2.09	91.8 : 3.21 : 6.89	72.7%
1 : 3	$(PbO)_{0.25}$ $(B_2O_3)_{0.75}$	0.25 : 1.5 : 2.5	100.36 : 3.47 : 7.28	51.7%

Moreover, in the Pb–B–O system, the glass forming range is very extensive, being sufficiently stable in the range of $PbO/B_2O_3 = 1/2$ to 4/1 (PbO content : 60 to 94 wt%).[17][18] Such a peculiar feature is observable otherwise only in Pb–Si–O glass. So the examinations of these glasses, being very interesting theme in the glass structure analysis itself, is expected to be very useful in understanding the structure of their melts.

From such reasons, we first of all have taken up this system and have carried out X-ray analysis of the glasses and melts in the range of $PbO/B_2O_3 = 4/1$ to 1/3.

a) Pb–B–O Glasses

Weighed powders of PbO and Boric-acid were mixed thoroughly, heated slowly in a platinum dish up to 1,000–1,300°C and kept at this temperature for 3–10 hours for completing dehydration. Then the dish was brought into contact with cold water and samples in the glassy state were obtained. Since the melt in the dish was only 2–4 mm in depth, the dehydration can be considered to be complete. When the content of PbO was large, the temperature was prevented from rising too high and the dish was covered in order to minimize the evaporation of PbO. The compositions of the obtained glass samples showed that the PbO contents agreed with the weighed values within the range of ± 2 wt%.

(17) J.E. Stanworth, "Physical Properties of Glass" (1950)
(18) A. Klemm and E. Berger, Glastech. Ber. **5** (1927/8), 405.

The X-ray scattering intensity curves of six samples having different compositions of pure B_2O_3 glass are given in Fig. 10. The gap between the curves of

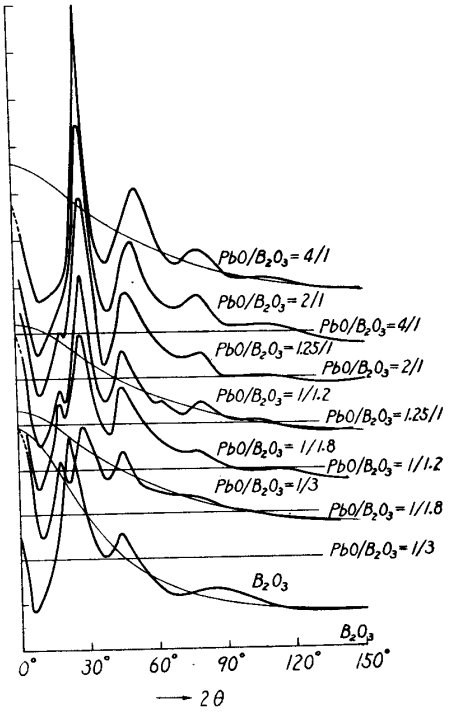

Fig. 10. X-ray scattering intensity curves of Pb-B-O glasses and B_2O_3 glass.

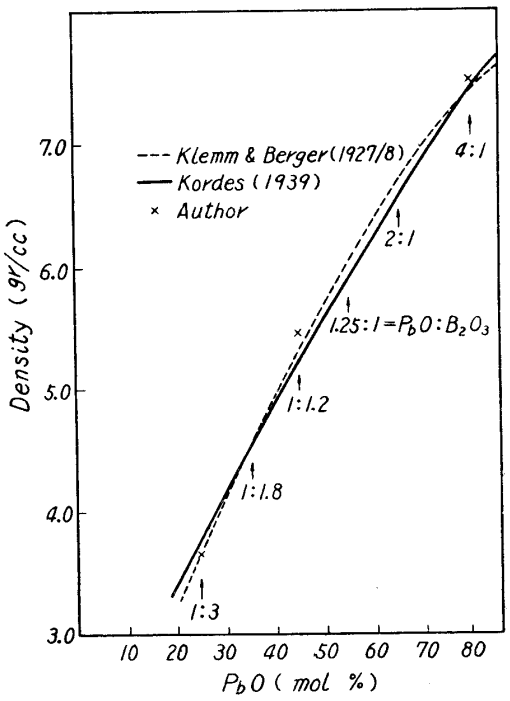

Fig. 11. Densities of Pb-B-O glasses.

pure B_2O_3 and glass of $PbO/B_2O_3=1/3$ being large, the correlation is not clear, but from other composition to the next can be seen a markedly continuous change, and we may conclude that the change in the structure is also continuous. This continuity may be also supported by the change in density shown in Fig. 11.[18][19]

Therefore we made more careful measurements on the samples of PbO/B_2O_3 =4/1, 1/1.2 and 1/3, and calculated their radial distribution curves, as shown by dotted lines in Figs. 13 to 18. Here, the absolute values are shown against onemol-equivalent. (For the related values, cf. Tab. 1.)

Crystal Structure of Pure PbO: The red crystal of low temperature type[20][12] is a tetragonal and layer structure as shown in Fig. 12, in which four oxygen atoms are collocated with a Pb atom, at the distance of 2.33Å. The yellow crystal of high temperature type is orthorhombic and nothing is known besides that it is of layer structure with oxygen atoms in every second interplaner space of the Pb layers similar as in the tetragonal above,

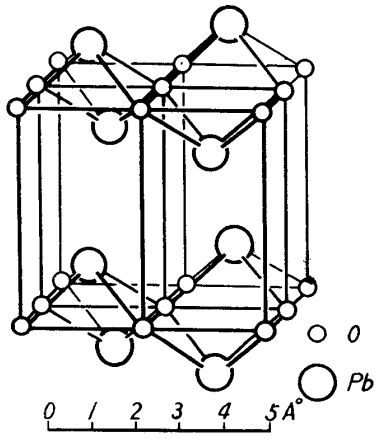

Fig. 12. Structure of tetragonal PbO crystal.

(19) E. Kordes, Z. Anorg. Allg. Chem. **241** (1939), 1.
(20) W.J. Moore and L. Pauling: J. Am. Chem. Soc. **63** (1941), 1392.

and that Pb–O distances are 2.20, 2.18 and 2.18Å respectively and O–O is 2.61Å[21], but the atomic distribution assumed from these data is not satisfactorily reconcilable with the curves in Fig. 16. On the contrary the tetragonal structure

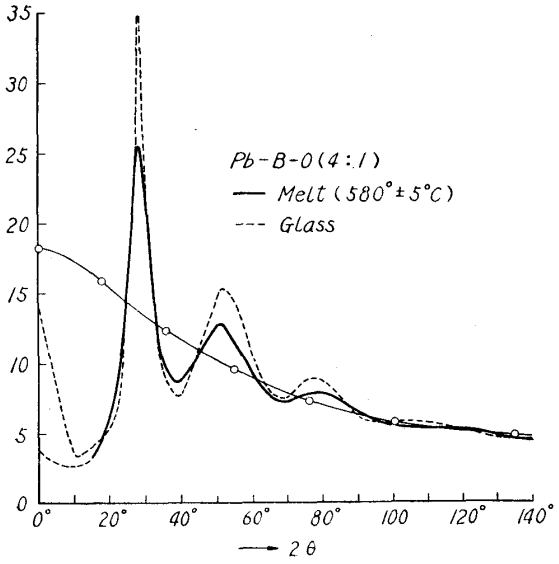

Fig. 13. X-ray scattering intensity curves of Pb–B–O (4 : 1) glass and melt

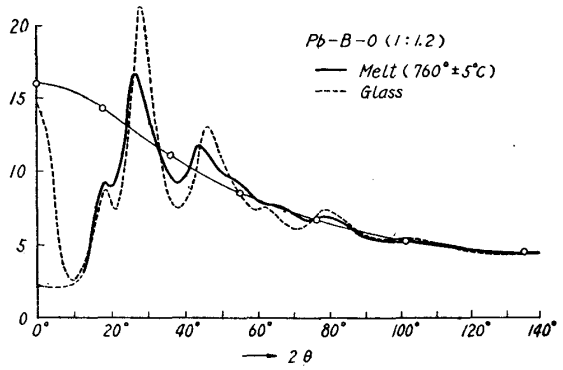

Fig. 14. X-ray scattering intensity curves of Pb–B–O(1 : 1.2) glass and melt.

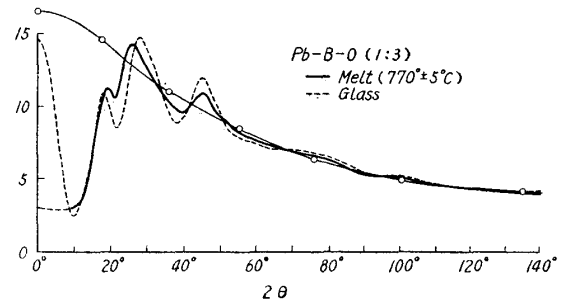

Fig. 15. X-ray scattering intensity curves of Pb–B–O (1 : 3) glass and melt.

coincide very well with them (cf. column graph in Fig. 16) that we took it as the basis of our discussions. This assumption must be subject to future rescrutiny. However, the ratio $\overline{K}_{Pb}/\overline{K}_0$ is here so large as to make the reliable crystal structure analysis impossible and the density of the yellow crystal, 9.2–9.5g/c.c., is not much different from that of the red, 9.53, so this assumption may be justified as not too unreasonable.

With such a structure of PbO crystal in mind and observing the radial distribution curves shown in Figs. 16 to 18 one by one, we may clearly grasp how the glass structure of 4 : 1 composition closely related to the PbO crystal gradually alters into that of normal borate glass. In the following, we will discuss this serial alteration.

The distances of the representative peaks and the typical components of the configurational model, ① to ⑩, are shown in Tab. 2.

First Peak: This is chiefly due to Pb–O. At the composition $PbO/B_2O_3=4/1$, the area of this peak reflects a coordination number of oxygen ions, 3.9, which resembles to that of the crystals, 4. With the increase of B_2O_3 content, this peak distance is elongated, thus approaching nearer to the pure ionic bond length of

(21) A. Byström, Arkiv. Kemi. Mineral Geol. **17B** (1943), 1; Chem. Ab. (1945),2018.

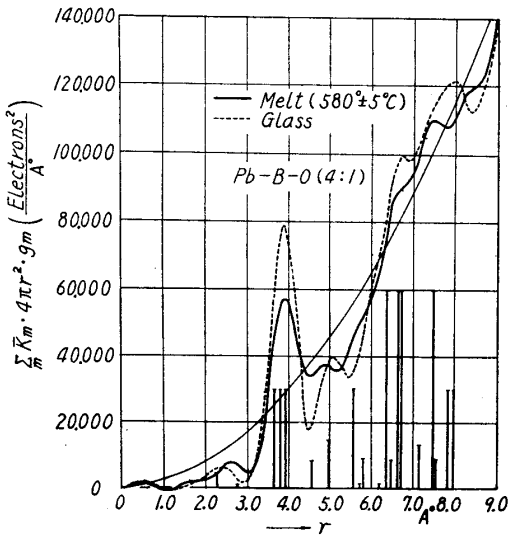

Fig. 16. Radial distribution curves of Pb-B-O (4 : 1) glass and melt.

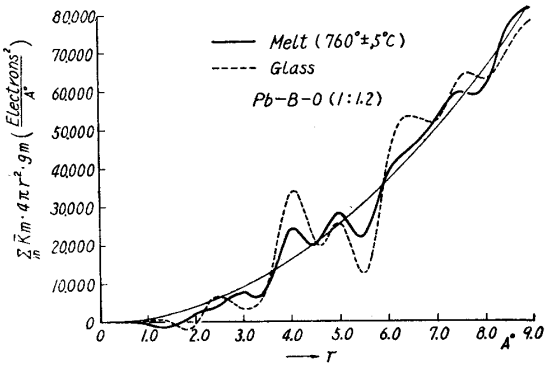

Fig. 17. Radial distribution curves of Pb-B-O (1 : 1.2) glass and melt.

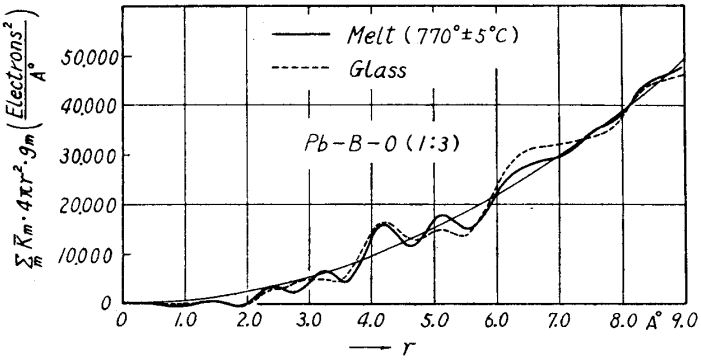

Fig. 18. Radial distribution curves of Pb-B-O (1 : 3) glass and melt.

Table 2. Peak-positions and configurational components of Pb-B-O glasses and melts

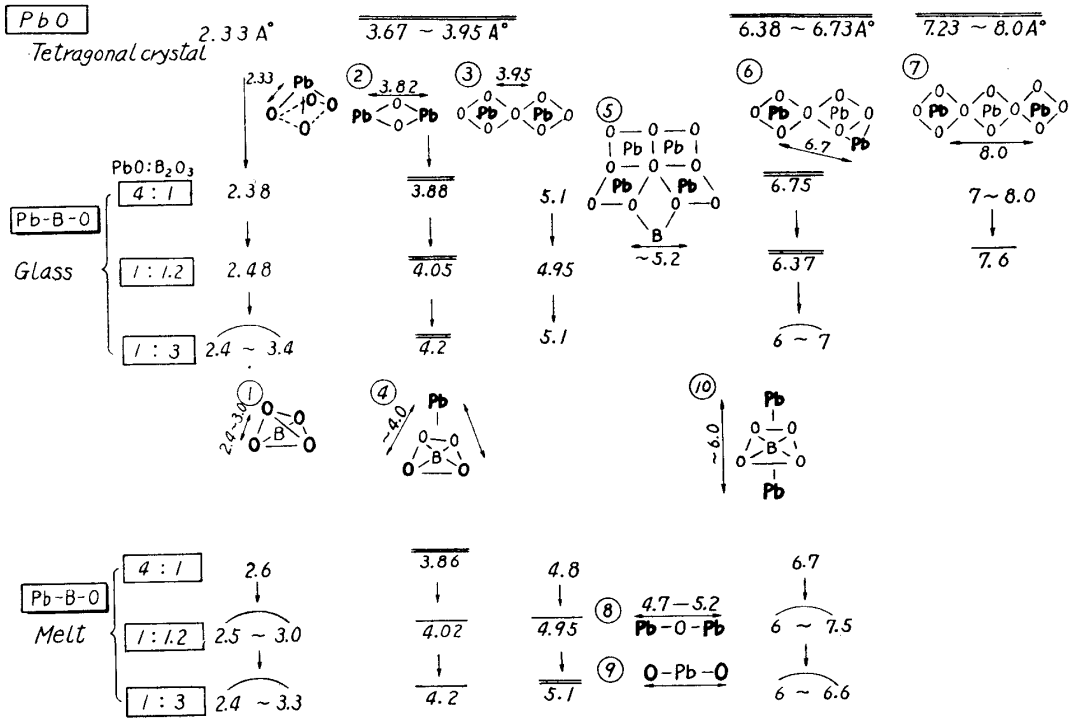

1.21Å+1.4Å=2.61Å from the semi-metallic bond length of 2.33Å in pure PbO, and so apparently showing that the PbO bond has more of the ionic character. This fact may be in correspondence with the tendency of lengthening of the other peak distance with the increase of B_2O_3 content. The extension of the first peak over 2.4 to 3.4Å at 1 : 3 composition may be due to the interference O–O in the borate tetrahedron. The length of O–O in pure B_2O_3 crystals is said to be 2.36–3.05Å.[22] Such a tetrahedron is illustrated as the model ① in Table 2.

Second Peak: This is a huge peak and can be explained without difficulty if we take it to be due to interference between two Pb ions with O ions as intermediary, as in the Models ② and ③. The area of the peak agrees with this explanation. When, however, content of B_2O_3 is further increased, Model ④ will also come into a play.

Third Peak: This peak located at 5Å or near is not so well outstanding, but in the range of large PbO contents, it corresponds with the Model ⑤ and reflects the part played by Boron as glass former. When the content of B_2O_3 is increased, the Models ⑧ and ⑨ concerned with free Pb^{++} and O^{--} ions may be supposed to come forth, too [cf. Next section, III (b)].

Fourth Peak: This large peak mainly corresponds to the Model ⑥ found also in pure PbO crystal. In this Model there are included Models ② and ③ corresponding to the second peak, as stated above. Some models besides ⑥ may be also considered as possible, for example, such as ⑩.

Fifth Peak: The Model ⑦ may be presumed here, which is consistent with Model ③. But the length is so large that a considerable bending may become possible, and a peak smaller than 8Å may occur. With decrease of the PbO content, this peak fades away.

Glass Forming Limit:[23] By combining the components of the configurational model observed in the above, we may explain the reason why the glass forming limit of this system is abnormal. As the four O–O edges of the PbO_4 quadrangular pyramid in a PbO crystal are all shared with one another, if we take N as the number of the PbO molecules, the total number of such edges will $4N/2=2N$ (cf. Fig. 12). By adding B_2O_3 to this, oxygen atoms may be entered into such layer-macromolecules, releasing the sharing of the edges. But introduction of a small quantity of oxygen will require an enormous energy, so that it would cause unstability. However, a three-dimensional network constructed by chain of PbO_4 pyramids will facilicate the formation of the stable glass structure. For this, about half of the number of sharing edges, N, should be freed. An atom of oxygen introduced at first will release two edges from sharing, but in the later stage one O atom coming in will release only one shared edge, so that the total number of oxygen atoms to be added for releasing N of O–O edges will amount 0.5 N to 1.0 N (mean value 0.75N). The experimentally known limit of glass-formation (83mol

(22) S.V. Berger, Acta Chem. Scand. **7** (1953), 611.
(23) G.W. Brady, J. Chem. Phys. **27** (1957), 300.

% or 94 wt% in PbO content) is near the composition of $PbO/B_2O_3=4/1$ in mol ratio and $Pb/O=1.75/1$ in atom ratio, corresponding to addition of about 0.75N of oxygen atoms, in good agreement with the above estimation*.

Such a chain of PbO_4-pyramids just corresponds to the Models ②, ③, ⑤, ⑥ and ⑦ in Tab. 2, probably strengthened by links of BO_3 and BO_4 tetrahedrons as shown in ⑤. When the B_2O_3 content is increased, a normal borate glass is obtained and its mechanical strength becomes abruptly greater. This is natural for the strength of B-O bond is more than twice that of Pb-O bond (cf. Tab. 3).

Table. 3. Bond-strength (Dissociation energy)

PbO : 145 Kcal/mol $\times\frac{1}{4}=38.2$ Kcal/mol	1
B_2O_3 : 712 " $\times\frac{1}{8}=89.2$ "	2.3

The peaks corresponding to these cases are as shown in the Models ①, ④, ⑧, ⑨ and ⑩ and happen to coincide with those of glass containing much PbO.

Tab. 4 shows the computed values of the density expected from simple packing of O^{--} and Pb^{++}. These values also suggest the specificity of 4 : 1 glass.

b) Fused Pb-B-O System

Now, how would the structure be changed when glasses of the above-stated structure are melted? The X-ray scattering curves of such melts near the melting point are shown in Figs. 13 to 15 by solid curves.

In general, the ripples are smaller than in the curves of glass, but the curves otherwise very similar, but in the curves of melts of 1 : 1.2 and 1 : 3 compositions some of the peaks are shifted to the side of smaller angles. This similarity is brought out more clearly when the radial distribution curves are calculated, for the peaks are here almost the same in their positions as those on the curves of glasses, only the relative height of them being varied (Figs. 16 to 18). Thus, these curves unequivocally sustain the interpretation that a glassy state is a state that occurs when a configurational structure of melt is supercooled and freezed.

The densities of melts just above the melting points were measured by a method using Pt pycnometer of special type, as shown in Table 4. For reference's sake, we will also show the densities of glasses (cf. Fig. 11) and the densities of melts measured by O'M. Bockris et al.[24] at 1,050°C in Table 4. As it is seen, thermal changes of density in this system contain some peculiar aspects or questions, but it seems that Bockris's data are less reliable. So we must do more precise measurements in future.

In the following, we will present some detailed discussions on the radial distribution curves of melts shown in Figs. 16 to 18. (cf. Table 2).

* I am now studying glassy and molten states of Pb-Si-O system in the range of $PbO/SiO_2=2.64/1\sim1/1.45$ in mol-ratio, too, and found that the radial distribution curve of the glass($PbO/SiO_2=2.64$ and 91wt% in PbO content) which corresponds to the glass-forming limit is very similar to that of Pb-B-O glass ($PbO/B_2O_3=4/1$). And in this case also Pb/O atom-ratio is equal to 1.75/1 supporting our above model.

(24) J. O'M. Bockris and G.W. Mellors, J. Phys. Chem. **60** (1956), 1321.

Table 4. Densities of Pb—B—O system (gr/c.c.)

	Calculated from (O^{--} = 17Å^3, Pb^{++} = 11Å^3)	Measured		
		Glass {Fig. 11) by Author	Melt	
			by author	from Ref. (24) at 1050°C.
PbO	13.2	(9.53)(crystal)		7.4
PbO : B_2O_3 4 : 1	9.3	7.45	7.12 (590°C)	6.7
1 : 1.2	5.72	5.45	5.23 (760°C)	5.5
1 : 3	3.97	3.66	3.38 (780°C)	4.3
B_2O_3	2.27	(1.84) (2.44)(crystal)		1.6

First Peak: We must note that the second peak being abnormally large, ghosts may appear in its vicinity; but in general, the distances of the first peak have lengthened over that in the case with glasses, so that it seems to approach nearer the ionic bond length 2.61 Å. The Pb-O bonds which can be generally considered apt to disrupt are apparently sundered in rather many instances in the melt, so that the melt becomes more ionic and of low viscosity. The fact that the electro-conductivity of such a melt at 1000°C is perfectly ionic[24] seems to support this inference.

Second and Third Peaks: The positions of these peaks are nearly the same as on the curves of glasses, but the relative heights of them are drastically changed, for when glass samples of high B_2O_3 contents are melted, the third peak becomes perceptibly larger than the second. This is perhaps owing to the preference in melts of the Models ⑧ and ⑨ containing free ionic Pb^{++} than to those of ②, ③ and ④ containing covalent bonds (see Fig. 19.). With the increase of the B_2O_3 content, that is, approaching the ideal ionic state, the third peak apparently shifts from 2×2.33Å$=4.66$Å to 2×2.6Å$=5.2$Å.

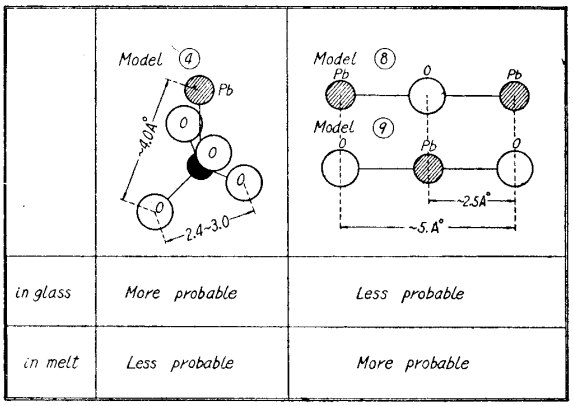

Fig. 19. Schematic representation of the difference of configurational structure in glass melt.

Fourth Peak: In the range above 6Å, the elevations of curves become lower and approach to the state of the mean distribution. This seems to suggest that in melts the configurational correlation in a large distance becomes enfeebled. But we may admit that the existence of model ⑩, which is proposed by WARREN et al.[1] in Na-Si-O glass, is here still posible. This means that the Model ④ is also included in Model ⑩.

In conclusion of the above discussion, we may state that the difference

between Pb–B–O glass and its melt consists in that, in the latter, the Pb–O bonds are sundered in a rather large number of instances, the atoms becoming more ionic and gaining in freedom. At the composition of 4 : 1, however, small groupings conforming to the Models ②, ③, ⑥ and ⑦ may be still sufficiently abundant, to cause a close similarity between the curves of glass and its melt. Moreover, it seems the existence of such small groups producing increase of the configurational entropy, and the energy required for cutting the bonds in them being small, the melting point of such glass is lowered very far (570°C) (cf. The section III (a) on $NaNO_3$). And the phase diagram in Fig. 12 shows that the melting point is further lowered at the composition close to 3 : 1. This phenomenon may be easily explained if we think that in such a case, $(PbO)_3$ (B_2O_3) is Pb_3 $(BO_3)_2$, so that nearly all the small BO_3 radicals may be more independent.

Summary

1. A new method of X-ray diffraction measurement widely applicable to fused materials including corrosive substances in the high temperature range has been described, in which the X-ray source and detector have been both rotated symmetrically against the free surface of the melt and the differentical-filters and the proportional counter with the pulse-height analyzer for the monochromation of X-rays have been used. And by the Fourier Analysis of X-ray diffraction data the atomic radial distribution curves of several fused materials have been obtained.

2. Fused $NaNO_3$ and $NaNO_2$ contain Na^+ ions and NO_3^- or NO_2^- radicals, which are in thermal motion having their specific coordinations determined by their specific shapes and charge distributions.

3. Such models are suitable for explaining the low melting points of these compounds.

4. The structure of Pb–B–O glasses and its abnormal glass-forming limit (83 mol% or 94 wt% in PbO content) were successfully explained by taking the tetragonal PbO crystal structure as the basis of discussion. Pb–O bond becomes more ionic by the increase of B_2O_3 content.

5. The radial distribution curves of the glass and its melt were in general essentially similar. Therefore it was verified that a glassy state is a state that occurs when a configurational structure of melt is supercooled and freezed.

6. The difference between the structure of Pb–B–O melts and of the glasses of the same composition lies in that by melting the Pb–O bonds are readily sundered and the atoms become more free ions.

Acknowledgment

The author is greatly indebted to Professor S. Takeuchi for his encouragement and support. Our hearty thanks are due to Professor Y. Morino, Dr. K. Kuchitsu and Mr. T. Iijima of the Faculty of Science, University of Tokyo for their valuable assistance in carrying out our FOURIER calculations.